Effects of substituent branching and chirality on the physical properties of ionic liquids based on cationic ruthenium sandwich complexes

Higashi, Tomomi
Ueda, Takahiro
Mochida, Tomoyuki

Effects of substituent branching and chirality on physical properties of ionic liquids based on cationic ruthenium sandwich complexes†

Tomomi Higashi, Takahiro Ueda, Tomoyuki Mochida*

An appropriate understanding of how substituents affect the physical properties of ionic liquids is important for the molecular design of ionic liquids. Toward this end, we investigated how the branching and chirality of substituents affects the physical properties of organometallic ionic liquids. We synthesized a series of ionic liquids bearing a branched or linear alkoxy group with the same number of carbons: $[Ru(C_5H_5)(\eta^6\text{-}C_6H_5OR)]X$ (*rac*-[**1**]X: R = $-CH(C_2H_5)(C_6H_{13})$, [**2**]X: R = $-CH(C_4H_9)_2$, [**3**]X: R = $-C_9H_{19}$), where X = PF_6^-, $(SO_2F)_2N^-$, and $(SO_2CF_3)_2N^-$. *rac*-[**1**]X are racemic salts. Salts with less symmetrical substituents tend to maintain the liquid state due to suppression of crystallization; crystallization is completely suppressed in most of *rac*-[**1**]X and in some of [**2**]X, whereas not in [**3**]X. The glass-transition temperatures and viscosities of the salts with branched substituents are greater than those with linear substituents. Chiral resolution of *rac*-[**1**][PF_6] was performed by chiral chromatography. The melting point of *rac*-[**1**][PF_6] is much lower than that of the enantiopure salt (*chiral*-[**1**][PF_6]), which we ascribe to the formation of a conglomerate in the solid state. X-ray structure analysis revealed that the solid salts form layered structures.

Department of Chemistry, Graduate School of Science, Kobe University, Kobe, Hyogo 657-8501, Japan. E-mail: tmochida@platinum.kobe-u.ac.jp

†Electronic supplementary information (ESI) available: DSC charts (Fig. S1), molecular structures of [**2**][PF_6] and [**3**][FSA] in the solid state (Fig. S2), viscosity data (Tables S1–S3), and crystallographic parameters (Table S4). CCDC-1403776 ([**2**][PF_6]), -1403774 ([**3**][PF_6]), and -1403775 ([**3**][FSA]) contain the supplementary crystallographic data. For ESI, see DOI: 10.1039/

Introduction

The science and technology of ionic liquids have attracted significant attention over this past decade.[1] Ionic liquids, which are salts with melting points below 100 °C, exhibit various characteristic properties such as nonvolatility, zero flammability, and high ionic conductivity. Elucidating the structure–property correlations of these materials is important for optimizing the molecular design of ionic liquids. Therefore, the effects of molecular structure, such as the length of alkyl substituents, on the physical properties of ionic liquids have been extensively investigated.[2,3] In this context, the effects of branched alkyl substituents are currently under active investigation.[4–11]

Although most ionic liquids contain organic cations such as imidazolium cations, various metal-containing ionic liquids that exhibit intriguing functionalities have recently been developed.[4,12–16] We previously synthesized organometallic ionic liquids from cationic sandwich complexes and studied their structure-property correlations, such as the effects of linear substituents and molecular symmetry.[17–21] We examine herein how substituent branching and chirality affect the thermal properties of organometallic ionic liquids. Although we use organometallic compounds because we have experience with these materials, the discussion hereafter also holds for general ionic liquids.

The effect of a branched substituent on the thermal properties of a molecular compound is an intriguing issue. Organic compounds with branched alkyl substituents often exhibit lower melting points,[22] lower glass-transition temperatures,[23] and lower isotropization temperatures[24] than those with the linear-chain substituents. Studies on metal-containing ionic liquids[4] and protonic ionic liquids[5] with branched alkyl substituents revealed that these compounds tend to exhibit lower glass-transition

temperatures and remain in the liquid state due to suppression of crystallization. Studies on imidazolium and triazolium ionic liquids revealed that the salts with branched substituents exhibit higher glass-transition temperatures[6] and higher viscosities[7–9] than those with linear substituents. However, while branched substituents often have chiral centers, relatively few studies have focused on how chirality affects the thermal properties of ionic-liquid-related materials.[25]

Chirality is an important issue in molecular compounds. A racemic mixture crystallizes either as a racemate, conglomerate, or solid solution, and these three racemic species have different thermal properties.[26] A racemate, or a racemic compound, constitutes an equal amount of left- and right-handed enantiomers regularly arranged in a crystal, whereas a conglomerate is a physical mixture of enantiopure crystals. Approximately 90% of organic crystalline racemic mixtures form racemates, 5–10% form conglomerates, and solid solutions are rare.[26] Recently, chiral ionic liquids have attracted significant attention owing to their applications in asymmetric synthesis, spectroscopy, and chromatography.[27] Therefore, elucidating the correlation between chirality and the thermal properties of ionic liquids is an important issue.

Herein, we contribute to this effort by reporting the synthesis and properties of organometallic ionic liquids with branched substituents (*rac*-[**1**]X, [**2**]X) or with linear substituents ([**3**]X) having the same number of carbon atoms as the branched substituents (Fig. 1). Bis(trifluoromethanesulfonyl)amide (= Tf_2N^-), bis(fluorosulfonyl)amide (= FSA^-), and hexafluorophosphate (= PF_6^-) were used as counter anions. The cation $[\mathbf{1}]^+$ has a chiral center in its substituent, and its salts are obtained as racemic mixtures (*rac*-[**1**]X). To separately discuss the effect of substituent branching and chirality, we performed chiral resolution of *rac*-[**1**]X by chiral chromatography to obtain *chiral*-[**3**]X, and investigated their thermal properties.

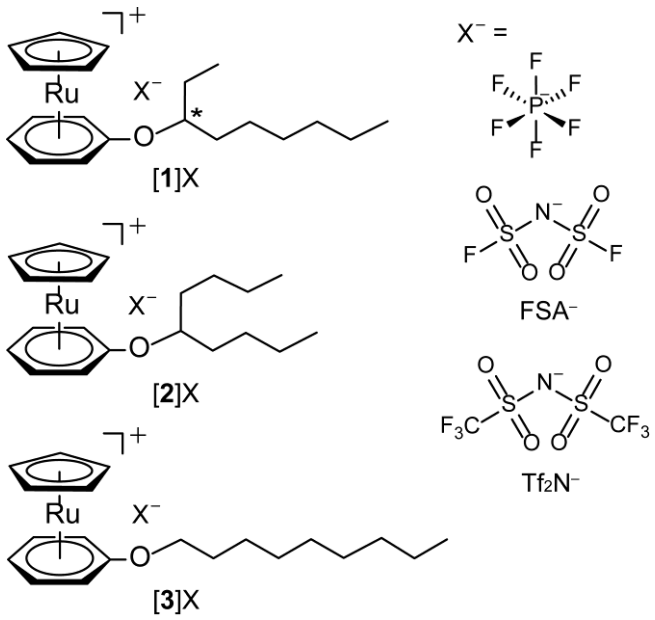

Fig. 1 Structural diagrams of the organometallic ionic liquids synthesized in this study ([**1**]X–[**3**]X). The * symbol in the [**1**]X diagram indicates the chiral center. The anion structures are shown on the right.

Results and Discussion

Synthesis

PF_6 salts were synthesized by reacting $[Ru(C_5H_5)(CH_3CN)_3][PF_6]$ and arene ligands (yields 52%–89%). FSA and Tf_2N salts were synthesized from the PF_6 salts by metathesis using K[FSA] and Li[Tf_2N], respectively (yields 38%–73%). The products were pale-yellow liquids or white solids with melting points below 100 °C. Chiral resolution of *rac*-[**1**][PF_6] was performed by chiral column chromatography, and part of the product was subjected to anion exchange. This procedure gave enantiotropically pure *chiral*-[**1**][PF_6] (>99.9% ee) and *chiral*-[**1**][FSA] (99.0% ee).

Thermal properties

Table 1 shows the melting points that were determined by differential scanning calorimetry (DSC), and the physical forms (solid or liquid) of the salts obtained at room temperature. A comparison of

these results reveals that the salts with branched substituents tend to remain in the liquid state to a greater extent than salts with linear substituents. The PF_6 salts were obtained as solids, except for *rac*-[**1**][PF_6], which scarcely solidified. Of the FSA salts, only [**3**][FSA] is a solid at room temperature, but [**2**][FSA] crystallizes at low temperature. The Tf_2N salts are liquids at room temperature, and [**3**][Tf_2N] crystallizes at low temperature. The cation dependence shows that the *rac*-[**1**]X salts are hard to crystallize, followed by [**2**]X, whereas [**3**]X crystallizes. This tendency indicates that lower-symmetry substituents render crystallization more difficult, allowing wider liquid temperature ranges. Concerning the anion dependence, the melting points decrease in the following order: PF_6 salts > FSA salts > Tf_2N salts, as is often observed in ionic liquids.

Table 1 Melting points (°C) and physical forms of as-obtained salts (*s*: solid, *l*: liquid).

X	*rac*-[**1**]X	*chiral*-[**1**]X	[**2**]X	[**3**]X
PF_6	42.4 (*l*)[a]	71.1 (*s*)	77.1 (*s*)	74.4 (*s*)
FSA	– (*l*)[c]	– (*l*)[c]	27.4 (*l*)[b]	57.9 (*s*)
Tf_2N	– (*l*)[c]		– (*l*)[c]	21.3 (*l*)[b]

[a]Not easily crystallized. [b]Crystallizes at low temperature. [c] Does not crystallize even at low temperature.

The glass-transition temperatures, melting points, and relevant thermodynamic parameters of the salts are listed in Table 2. Their comparison suggests that the salts with branched substituents (*rac*/*chiral*-[**1**]X and [**2**]X) generally have a glass-transition temperature approximately 10 °C higher than that of a linear-chain derivative ([**3**]X). This result is consistent with the higher viscosity of the salts with branched substituents (*vide infra*). Nearly half of the salts exhibit both a melting point and a glass transition, and the ratios T_g/T_m are close to 2/3 (Table 2), as generally seen for molecular liquids.[28,29] The high T_g/T_m ratio for [**2**][FSA] may be attributed to its high-energy packing in the solid state. For *rac*-[**1**][PF_6], the origin of the high T_g/T_m ratio is discussed in the following section. Note that *chiral*-[**1**]X and *rac*-[**1**]X have almost the same T_g, which is 1 K lower in the chiral salt for both PF_6 and FSA salts.

Ionic liquids from cationic sandwich complexes often undergo phase transitions in the solid state.[17] For the present salts, only [**2**][PF_6] and [**3**][Tf_2N] exhibit phase transitions in the solid state. [**2**][PF_6] exhibits a phase transition at 70.1 °C (ΔS = 18.8 J mol^{-1} K^{-1}). [**3**][Tf_2N] exhibits a phase transition at –14.4 °C (ΔS_m = 41.9 J mol^{-1} K^{-1}) to a plastic phase (T_m = 22.4 °C, ΔS_m = 1.3 J mol^{-1} K^{-1}), and heating the plastic phase at a slow rate results in an exothermic transition to a nonplastic phase (T_m = 21.3 °C, ΔS_m = 79.9 J mol^{-1} K^{-1}) (Fig. S1(g), ESI).

The melting entropies of *rac/chiral*-[**1**]X and [**2**]X (55–64 J mol^{-1} K^{-1}), including the contribution of the solid phase transition for [**2**][PF_6], are smaller than those of [**3**]X, which has linear substituents (80–106 J mol^{-1} K^{-1}). This feature reflects the fact that branched alkyl substituents have less conformational freedom than linear substituents.

Table 2 Glass-transition temperature T_g, melting point T_m, melting entropy ΔS_m, melting enthalpy ΔH_m, and decomposition temperature T_{dec} for the salts synthesized in this study.

	T_g (°C)	T_m (°C)	ΔH_m (kJ mol^{-1})	ΔS_m (J mol^{-1} K^{-1})	T_g (K) / T_m (K)	T_{dec} (°C)[a]
PF_6 salts						
rac-[**1**][PF_6]	–35	42.4	17.3	53.8	0.76	
chilal-[**1**][PF_6]	–36	71.1	22.0	63.5	0.69	
[**2**][PF_6]		77.1	12.6	35.9		
[**3**][PF_6]	–45	74.4	32.2	92.4	0.66	
FSA salts						
rac-[**1**][FSA]	–61					265
chiral-[**1**][FSA]	–62					
[**2**][FSA]	–58	27.4	15.8	52.1	0.72	260
[**3**][FSA]		57.9	35.5	106.4		276
Tf_2N salts						
rac-[**1**][Tf_2N]	–60					277

[**2**][Tf_2N]	–56					272
[**3**][Tf_2N]	–70	21.3	23.7[b]	79.9[b]	0.69	330

[a] Decomposition temperatures determined by TG analysis. (–3%wt, 10 K/min). [b] Melting enthalpy and entropy of stable phase.

Correlation between chirality and melting points

Because all PF_6 salts used herein have melting points, we examined how their substituent chirality and branching affects their melting point. As shown in Table 1, *rac*-[**1**][PF_6] has a much lower melting point (T_m = 42.4 °C) than *chiral*-[**1**][PF_6] and the other salts (T_m = 71.1–77.4 °C). To elucidate the origin of the low melting point, we examined the melting behavior of mixtures of *chiral*-[**1**][PF_6] and *rac*-[**1**][PF_6] with different mixing ratios. Figure 2 shows the resulting solid-liquid phase diagram plotted as a function of enantiomeric excess (ee); this result is typical of a conglomerate system. The system has a eutectic temperature that matches the melting point of the racemic salt, and the theoretical liquidus line based on the Schröder–Van Laar equation [$\ln(x) = \Delta H_m/R(1/T_m–1/T)$][26] is in excellent agreement with the observed data. The values of ΔH_m and $T_{m(peak)}$ for *chiral*-[**1**][PF_6] were used to calculate the liquidus line. In addition, the powder-X ray patterns of *chiral*-[**1**][PF_6] and *rac*-[**1**][PF_6] were the same. These results demonstrate that the racemic salt forms a conglomerate in the solid state, which consists of a physical mixture of enantiopure crystals.[26] Therefore, we conclude that the entropy of mixing causes the lower melting point of the racemic salt.

The high T_g/T_m ratio for *rac*-[**1**][PF_6] (0.76, see Table 2) is consistent with this phenomenon: its low melting point is caused by the entropy of mixing, whereas its glass transition-temperature is comparable to that of the enantiopure salt. On the basis of these results, we conclude that the melting points of these salts are essentially comparable regardless of whether the salts have linear or branched substituents, whereas mixing enantiomers lowers the melting point of the racemic salt. The formation of a conglomerate by *rac*-[**1**][PF_6] also accounts for its resistance to crystallization. Although *chiral*-[**1**][PF_6] easily crystallizes at room temperature, *rac*-[**1**][PF_6] only crystallizes at low temperature and

with repeated mechanical perturbation. In the racemic salt, effective formation of chiral crystal nuclei is probably inhibited due to the presence of the opposite enantiomers.

The effects of chirality and branching have yet to be considered separately in studies of ionic liquids. This study shows that because of the entropy of mixing, the melting point of a racemic ionic liquid can be much lower than that of a chiral ionic liquid. These results suggest that the effects heretofore ascribed to branched substituents, such as a lower melting point or stabilization of the liquid state, may be at least partly ascribed to the entropy of mixing rather than to the branching itself.

The thermal behavior of mixtures of different ionic liquids, however, has been reported, with the conclusion being that mixing cations often leads to a lower melting point or suppression of crystallization.[30,31] Our study has shown that the use of racemic mixtures can be a useful strategy to lower the melting point of an ionic liquid while maintaining its chemical composition. Note, however, that this strategy is not always effective because if a racemic mixture crystallizes as a racemate, its melting point can be higher than that of the enantiopure crystal,[26] especially when the interaction is stronger between opposite enantiomers. In fact, in several chiral imidazolium salts, the racemic salts have higher melting points than the enantiopure salts.[25]

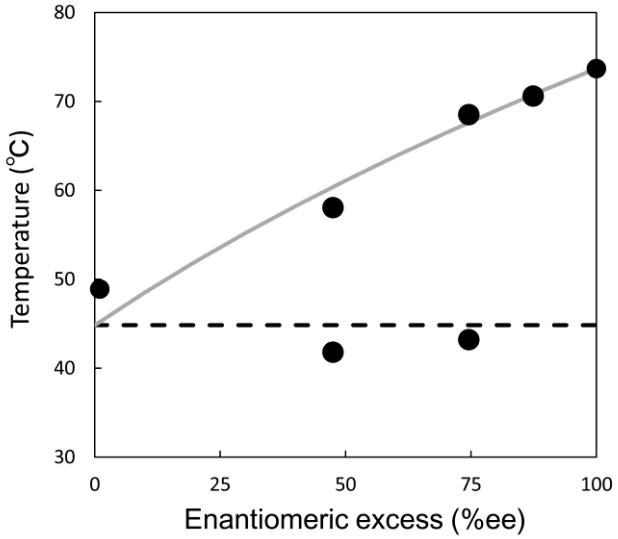

Fig. 2 Solid–liquid phase diagram of *rac*/*chiral*-[**1**][PF_6] plotted in the form of temperature vs enantiomeric excess. The gray line is the theoretical liquidus line calculated using the Schröder–Van

Laar equation and the dotted line represents the eutectic temperature.

Thermogravimetric analysis

The thermal decomposition temperatures of FSA salts and Tf_2N salts were investigated by thermogravimetric (TG) analysis; the results show that salts with branched substituents are thermally less stable than those with linear substituents. The decomposition temperatures (T_{dec}, −3wt%) of the salts are given in Table 2, and TG curves are shown in Fig. 3. The salts with branched substituents, *rac*-[**1**]X and [**2**]X, have almost identical TG curves, and their decomposition temperatures (*rac*-[**1**]X: 265 °C for X = FSA^-, 277 °C for X = Tf_2N^-; [**2**]X: 260 °C for X = FSA^-, 272 °C for X = Tf_2N^-) are lower than those of [**3**]X (276 °C for X = FSA^- and 330 °C for X = Tf_2N^-) with the same anion.

Concerning the anion dependence, the Tf_2N salts are thermally more stable than the FSA salts because of the higher thermal stability of Tf_2N^-.[32] This feature allowed us to observe the decomposition of the cations in the Tf_2N salts. As seen in Fig. 3b, the Tf_2N salts undergo a two-step mass loss. The first step (approximately 20% mass loss) corresponds to the dissociation of the alkyl moiety from the cation (calc. 19.1%) associated with dissociation of the ether bond. The secondary radicals formed by dissociation of the branched substituents are more stable than the primary radicals that form upon dissociation of the linear substituents. This feature explains the lower decomposition temperature of salts with branched substituents.

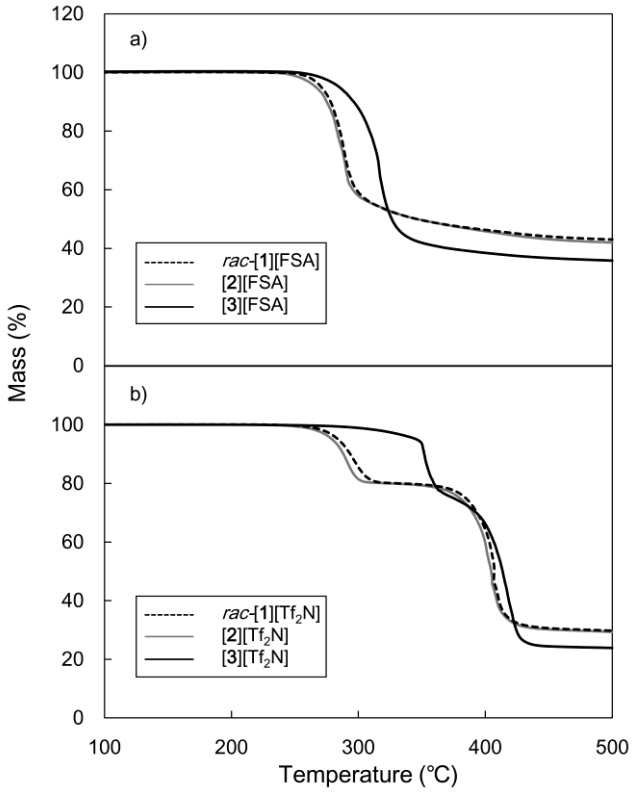

Fig. 3 Thermogravimetric traces of (a) FSA salts and (b) Tf_2N salts (10 K min^{-1}).

Viscosities

We measured the viscosities of the liquid samples, *rac*-[**1**]X (X = PF_6^-, FSA^-, Tf_2N^-), [**2**]X (X = FSA^-, Tf_2N^-), and [**3**][Tf_2N] and found that salts with branched substituents tend to have a higher viscosity than those with linear substituents. The viscosity data at 25 °C and relevant parameters derived from the Arrhenius plot and Vogel–Fulcher–Tammann (VFT) approximation are listed in Table 3. The viscosities at room temperature (310–1100 mPa s for FSA and Tf_2N salts) are much higher than those of imidazolium-based ionic liquids (cf. [Bmim][Tf_2N]: 49 mPa s).[33] Figure 4 shows the viscosities plotted as functions of temperature. Viscosity data are summarized in Tables S1–S3 (ESI).

The viscosity of the Tf_2N salts at room temperature increases in going from [**3**][Tf_2N] (312 mPa s) to *rac*-[**1**][Tf_2N] (623 mPa s) to [**2**][Tf_2N] (775 mPa s). FSA salts also exhibit the tendency *rac*-[**1**][FSA] (700 mPa s) < [**2**][FSA] (1107 mPa s). These results indicate that the viscosity increases with

increasing bulkiness of the substituents. This tendency is consistent with previous reports that the viscosity of ionic liquids with branched substituents are generally greater than for ionic liquids with linear substituents,[7,8] owing to the more stable packing between cations and anions.[9] Concerning the anion dependence, the viscosities of the FSA salts are greater than those of the Tf_2N salts with the same cation. This result is exceptional because the viscosity of FSA salts at room temperature is usually less than that of Tf_2N salts.[34–36] However, the activation energies E_a of the FSA salts are less than those of the Tf_2N salts; thus, the viscosities of the FSA salts should be less at low temperatures. This is consistent with the glass-transition temperatures of the FSA salts, which are slightly less than those of the Tf_2N salts.

The present liquids are more viscous than the related ionic liquids with a shorter butyl substituent $[Ru(C_5H_5)(\eta^6\text{-}C_6H_5{}^n\text{Bu})]X$ (η = 91 mPa s for X = FSA^-, 137 mPa s for X = Tf_2N^-)[20] and the activation energies E_a derived from the Arrhenius plots [$\eta = \eta_0 e^{(Ea/RT)}$] are also greater (see Table 3). This result is ascribed primarily to the greater length of the substituent.[2] The data were fit using the VFT equation ($\eta = \eta_0 e^{[DT_0/(T-T_0)]}$), where T_0 is the ideal glass-transition temperature and D is a parameter that reflects the deviation from Arrhenius behavior.[37] For these experiments, D falls in the range 12.7–19.8, which is greater than that of $[Ru(C_5H_5)(\eta^6\text{-}C_6H_5{}^n\text{Bu})]X$ (D = 6.5 for X = FSA^-, 5.6 for X = Tf_2N^-).[20] An increase in D for longer substituents is also observed in alkylimidazolium ionic liquids[2] and in ferrocene-based ionic liquids.[38]

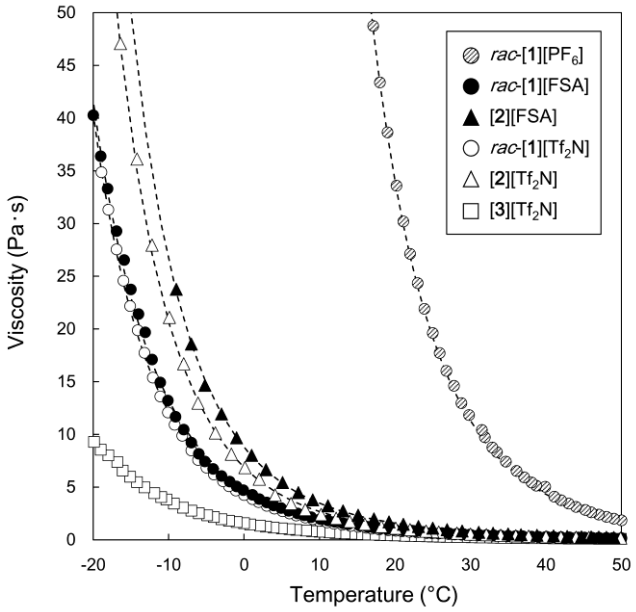

Fig. 4 Viscosity as a function of temperature for *rac*-[**1**]X, [**2**]X, and [**3**]X (X = PF_6^-, FSA^-, Tf_2N^-).

Table 3 Viscosity data and relevant parameters for liquid samples.

	$\eta_{25\,°C}$ (mPa s)	E_a (kJ mol^{-1})	D	η_0 (mPa s)	T_0 (°C)
rac-[**1**][PF_6]	19600	80.1	12.7	5.6×10^{-3}	–111
rac-[**1**][FSA]	700	52.5	19.8	2.1×10^{-3}	–157
[**2**][FSA]	1107	55.3	8.1	9.5×10^{-2}	–113
rac-[**1**][Tf_2N]	623	53.6	13.1	9.3×10^{-3}	–137
[**2**][Tf_2N]	775	59.0	10.2	2.6×10^{-2}	–123
[**3**][Tf_2N]	312	44.5	13.2	1.8×10^{-2}	–147
[Ru(C_5H_5)(η^6-$C_6H_5{}^n$Bu)][FSA][a]	91	29.8	6.5	0.21	–131
[Ru(C_5H_5)(η^6-$C_6H_5{}^n$Bu)][Tf_2N][a]	137	35.8	5.6	0.22	–115
[Bmim][Tf_2N][b]	49	31.3	4.7	0.25	–109

[a] Reference 20. [b] Reference 33 (Bmim = 1-butyl-3-methylimidazolium cation).

Crystal structures

The crystal structures of [**2**][PF_6], [**3**][PF_6], and [**3**][FSA] were determined by X-ray crystallography with the samples at −173 °C; the results reveal the formation of lamellar structures in these salts. Each salt belongs to the space group *P*–1. Ortep drawings of the molecular structure in [**2**][PF_6] and [**3**][FSA]

are shown in Fig. S2 (ESI). Two crystallographically independent cations are detected in [**2**][PF_6], one of which exhibits two-fold disorder (0.5:0.5) of the alkyl chain. The alkyl substituents in [**3**][PF_6] and [**3**][FSA] take on the all-*trans* conformation. In the sandwich moieties, the Ru–C bond involving the carbon atom with the alkoxy substituent is longer than the other Ru–C_{arene} bonds, which means that the cyclopentadienyl (Cp) and arene rings are canted (dihedral angles of 0.5°–4.8°), as often seen in related salts.[20]

Figure 5 shows the packing diagrams of the salts, which consist of lamellar structures composed of cation–anion ionic layers and alkyl-chain layers. The alkyl chains in [**3**][PF_6] and [**3**][FSA] are aligned parallel to each other. This structure contrasts that of the sandwich complexes [Ru(C_5H_5)(C_6H_5R)]X that have heteroatoms in their substituents,[20] wherein layered structures do not form because of hydrogen-bond-like interactions between the heteroatoms and the hydrogens on the cation.

Intermolecular cation–anion short contacts are present in the ionic layers. In [**2**][PF_6] and [**3**][PF_6], these short contacts appear between the ring hydrogens and the fluorine or oxygen atoms (CH_{arene}···F), which are 0.2–0.3 Å shorter than the van der Waals contact distances. [**3**][FSA] has short contacts between the arene hydrogens and the oxygen atoms in the anion (CH_{arene}···O distance: 2.29 Å), which were 0.4 Å shorter than the van der Waals distance. Such cation–anion interatomic contacts often appear in crystals of ionic liquids from sandwich complexes.[18,20] Moreover, π–π contacts exist between the Cp rings (closest C···C distance is 3.29 Å) in [**2**][PF_6] and between the arene and Cp rings (closest C···C distance is 3.18 Å) in [**3**][FSA]. However, [**3**][PF_6] exhibits no such π–π interaction.

The density of [**2**][PF_6] (1.606 mg m^{-3}) determined crystallographically at −173 °C is less than that of [**3**][PF_6] (1.622 mg m^{-3}); this is a result that we ascribed to the presence of disorder. However, the melting point of [**2**][PF_6] (77.1 °C) is higher than that of the more densely packed [**3**][PF_6] (74.4 °C). This phenomenon is probably related to the large disorder in [**2**][PF_6] in the high-temperature phase (*vide ante*), which thermodynamically stabilizes the solid phase.

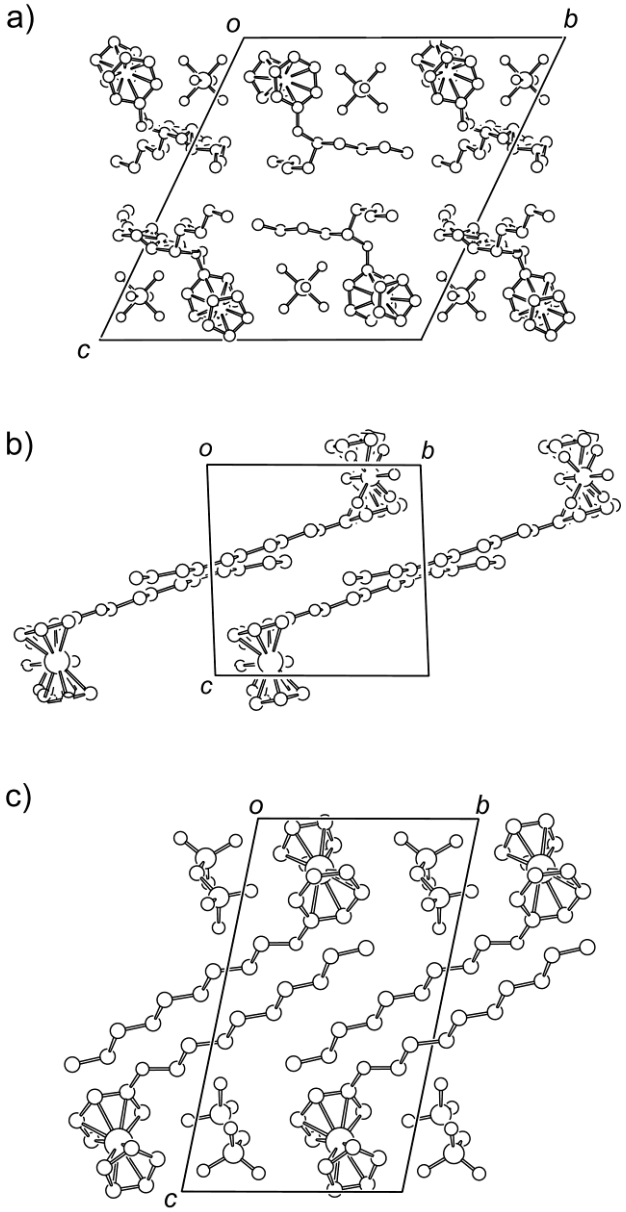

Fig. 5 Packing diagrams of (a) [**2**][PF_6], (b) [**3**][PF_6], and (c) [**3**][FSA]. Hydrogen atoms are omitted for clarity.

Conclusion

We investigated how substituent branching and chirality affects the physical properties of ionic liquids containing cationic sandwich complexes. Ionic liquids with branched [–OCH(C_2H_5)(C_6H_{13}), –OCH(C_4H_9)$_2$], or linear (–OC_9H_{19}) substituents were prepared, and the results of experiments indicate

that the crystallization of salts with substituents of lower symmetry is more likely to be suppressed. The viscosity and glass-transition temperature increase with increasing bulkiness of the substituent. In the case of the PF_6 salts with the chiral branched substituent [–$OCH(C_2H_5)(C_6H_{13})$], the melting point of the racemic salt is much lower than that of the enantiopure salt. This phenomenon is ascribed to the formation of a conglomerate of the racemic salt in the solid state, which lowers the melting point due to the contribution of the entropy of mixing.

These experiments elucidate independently the effect of substituent chirality and branching via chiral resolution of the racemic salt. The results suggest that effects considered in previous studies to result from substituent branching, such as a reduced melting point and stabilization of the liquid state, may at least partly be ascribed to the effect of chirality instead of being ascribed only to substituent branching. Although this study uses organometallic ionic liquids, the effects of branched substituents observed herein should provide useful knowledge for the molecular design of various ionic liquids. For example, the use of a racemic mixture is revealed to be a useful method to lower the melting point of ionic liquids. This is advantageous also because racemic molecules are generally easy to synthesize. However, note that this strategy is not always effective because the melting point may increase if a racemate is formed instead of a conglomerate.

Experimental

General

$[Ru(C_5H_5)(CH_3CN)_3][PF_6]$ was prepared following the literature.[39] ^1H NMR spectra were recorded using a JOEL JNM-ECL-400 spectrometer or a Bruker Avance 400 spectrometer. Elemental analyses were done on a PerkinElmer 2400II elemental analyzer. DSC measurements were performed using a TA Q100 differential scanning calorimeter at a scan rate of 10 K min^{-1}, and other rates were applied as required. DSC measurements on the mixtures of the racemic and chiral salts were done on samples that had been heated once to 105 °C to homogeneously mix the components in the liquid state;

following this they were stored at −10°C for one month to allow them to crystallize. Peak-maximum temperatures were used to produce the phase diagram because peak-onset temperatures were difficult to determine. TG analysis was performed using a Rigaku TG8120 with the samples under a nitrogen atmosphere. FT-IR spectra were acquired via attenuated total reflectance (ATR) using a Thermo Scientific Nicolet iS5 spectrometer. Viscosities of liquids were measured with a Toki Sangyo TV-22L viscometer using a 3 R7.7 cone rotor. The VFT fitting was performed using a non-linear least-square method, implemented in the IGOR Pro software program, which is based on the Levenberg-Marquardt algorithm. The ionic liquids were dried under vacuum at 80 °C overnight before the viscosities were measured. Powder X-ray diffraction measurements for *rac*-[**3**][PF_6] and *chiral*-[**3**][PF_6] were performed by using Rigaku SmartLab and Bruker APEX II Ultra diffractometer.

Synthesis of ligands

(1-Butylpentyl)oxy-benzene. Under a nitrogen atmosphere, phenol (0.94 g, 10 mmol), 5-nonanol (2.1 mL, 12 mmol), triethylamine (1.4 mL, 10 mmol), and PPh_3 (2.62 g, 10 mmol) were dissolved in dry tetrahydrofuran (6.8 mL). The solution was cooled to 0 °C, and then diisopropyl azodicarboxylate (40% in toluene; 5.3 mL, 10 mmol) was added dropwise. The reaction mixture was stirred at room temperature for one day. The reaction mixture was quenched with 5% HCl (10 mL) and extracted with diethyl ether. Evaporation of the ether solution gave a liquid. Addition of hexane to the liquid led to a white solid precipitate, which was removed by filtration. Evaporation of the filtrate provided a colorless liquid. This procedure was repeated until no precipitation occurred. The product was purified by column chromatography [silica gel, eluent: hexane/dichloromethane (2:1, v/v), R_f = 0.5]. The desired compound was obtained as a colorless liquid and used for the subsequent step after vacuum drying for 3 h (1.22 g, 56% yield). ^{1}H NMR (400 MHz, $CDCl_3$): δ = 0.89 (t, 6H, CH_3, J = 7.0 Hz), 1.26–1.47 (m, 8H, CH_2), 1.56–1.69 (m, 4H, CH_2), 4.01 (quint, 1H, CHBr, J = 5.9 Hz), 6.87–6.92 (m, 3H, Ar–H_3), 7.24–7.28 (m, 2H, Ar–H_2).

(1-Ethylhexyl)oxy-benzene. This compound was synthesized as described for [(1-butylpentyl)oxy]benzene, using phenol (0.94 g, 10 mmol), 3-nonanol (2.1 mL, 12 mmol), trimethylamine (1.4 mL, 10 mmol), PPh_3 (2.62 g, 10 mmol) and dry tetrahydrofuran (6.8 mL). The product was obtained as a colorless liquid (1.04 g, 47% yield). ^{1}H NMR (400 MHz, $CDCl_3$): δ = 0.87 (t, 3H, C*H*$_3$, *J* = 7.0 Hz), 0.95 (t, 3H, C*H*$_3$, *J* = 7.6 Hz), 1.26–1.47 (m, 4H, C*H*$_2$), 1.55–1.70 (m, 4H, C*H*$_2$), 4.15 (quint, 1H, ArOC*H*, *J* = 5.8 Hz), 6.87–6.92 (m, 3H, Ar–*H*$_3$), 7.22–7.28 (m, 2H, Ar–*H*$_2$).

Nonyloxybenzene. Under a nitrogen atmosphere, phenol (500 mg, 5.31 mmol), potassium carbonate (1.38 g, 10 mmol), and 18-crown-6 (119 mg, 0.36 mmol) were dissolved in dimethylformamide (12 mL). 1-Bromononane (1.2 mL, 5.8 mmol) was added to this solution, and the mixture was stirred and maintained at 80 °C for 28 h. The reaction mixture was poured onto cold water and extracted five times with a mixture of ethyl acetate and hexane (1:1 v/v). The desired product was obtained as a white solid by recrystallization from methanol (−40 °C), which was collected by decantation at low temperature (698 mg, 59% yield). This compound—a colorless liquid at room temperature—was used for the subsequent step after vacuum drying for 3 h. ^{1}H NMR (400 MHz, $CDCl_3$): δ = 0.88 (t, 3H, C*H*$_3$, *J* = 6.8 Hz), 1.29–1.34 (m, 10H, C*H*$_2$), 1.41–1.48 (m, 2H, C*H*$_2$), 1.77 (quint, 2H, C*H*$_2$, *J* = 7.1 Hz), 3.94 (t, 2H, C*H*$_2$, *J* = 6.6 Hz), 6.87–6.94 (m, 2H, Ar–*H*$_2$), 7.24–7.30 (m, 3H, Ar–*H*$_3$).

Synthesis of [Ru(C_5H_5){η^6-$C_6H_5OCH(C_2H_5)(C_6H_{13})$}]X ([1]X; X = PF_6^-, FSA^-, Tf_2N^-)

[Ru(C_5H_5){η^6-$C_6H_5OCH(C_2H_5)(C_6H_{13})$}][$PF_6$] (*rac*-[1][$PF_6$] and *chiral*-[1][$PF_6$]). Under a nitrogen atmosphere, (1-ethylhexyl)oxy-benzene (404 mg, 1.83 mmol) was added to a solution of [Ru(C_5H_5)(CH_3CN)$_3$][PF_6] (666 mg, 1.53 mmol) in acetonitrile (10 mL), and the solution was maintained at 90 °C for 24 h. Next, the solvent was evaporated, and the residue suspension in toluene

was passed through a short plug of alumina (eluent: toluene and then acetonitrile). After evaporation of the solvent, the residue was dissolved in acetonitrile and washed three times with hexane. The product was dried under vacuum at 80 °C for 15 h. This pale yellow liquid solidified after storing overnight at 10 °C with repeated stimulus applied with a spatula, giving a white solid (421 mg, 52% yield). ^{1}H NMR (400 MHz, $CDCl_3$): δ = 0.88 (t, 3H, C*H*$_3$, *J* = 6.4 Hz), δ = 0.95 (t, 3H, C*H*$_3$, *J* = 7.4 Hz), 1.19–1.35 (m, 8H, C*H*$_2$), 1.61–1.72 (m, 4H, C*H*$_2$), 4.18 (quint, 1H, ArOC*H*), 5.33 (s, 5H, Cp–*H*$_5$), 5.91–5.94 (m, 1H, Ar–*H*$_1$), 6.07–6.15 (m, 4H, Ar–*H*$_4$). IR (ATR, cm^{-1}): ν = 1256, 823, 556. Anal. Calcd. for $C_{20}H_{29}F_6OPRu$: C,45.20; H, 5.50; N, 0.00. Found: C, 45.11; H, 5.45; N, 0.14. Chiral resolution of *rac*-[**1**][PF_6] was performed by high-performance liquid chromatography (HPLC) by using a chiral column (column: YMC CHIRAL ART Amylose-C). The mobile phase consisted of methanol containing 0.1% trifluoroacetic acid and 0.1% diethylamine. The first fraction was collected and concentrated under reduced pressure. To remove additives, anion exchange using KPF_6 was performed in water, and extraction with dichloromethane gave the chiral compound *chiral*-[**1**][PF_6] (> 99.9% ee, HPLC) at approximately 50% yield. The product was dried at 80 °C under vacuum for 15 h, and an elemental analysis yielded satisfactory data. The second fraction containing the other enantiomer (99.0% ee, HPLC) was used to synthesize the FSA salt, as described in the following section.

[Ru(C_5H_5){η^6-$C_6H_5OCH(C_2H_5)(C_6H_{13})$}][FSA] (*rac*-[1][FSA] and *chiral*-[1][FSA]). [Ru(C_5H_5){η^6-$C_6H_5OCH(C_2H_5)(C_6H_{13})$}][$PF_6$] (162 mg, 0.30 mmol) was dissolved in a mixture of water and acetone. An aqueous solution of K[FSA] (200 mg, 0.91 mmol) was added to this solution that was stirred for 5 min. After evaporation of the acetone, the resulting suspension was extracted five times with dichloromethane, and the organic layer was washed 10 times with water. Next, the product was dissolved in dichloromethane and treated with activated carbon. The product was dispersed in toluene by ultrasonic agitation and passed through a short plug of alumina (eluent: toluene and then

acetonitrile). The desired compound was obtained as a pale yellow liquid, which was dried at 80 °C under vacuum for 15 h (121 mg, 70% yield). ^{1}H NMR (400 MHz, $CDCl_3$): δ = 0.93 (t, 6H, CH_3, J = 7.0 Hz), 1.25–1.36 (m, 8H, CH_2), 1.61–1.66 (m, 4H, CH_2), 4.21–4.24 (m, 1H, ArOCH), 5.33 (s, 5H, Cp–H_5), 5.91 (t, 1H, Ar–H_1, J = 5.0 Hz), 6.10–6.14 (m, 4H, Ar–H_4). IR (ATR, cm^{-1}): ν = 1378, 1362, 1257, 1178, 1102, 824, 737, 568. Anal. Calcd. for $C_{20}H_{29}F_2NO_5RuS_2$: C, 42.39; H, 5.16; N, 2.47. Found: C, 42.61; H, 5.42; N, 2.43. *chiral*-[**1**][FSA] (99.0% ee) was prepared from *chiral*-[**1**][PF_6] by the same procedure at a yield of approximately 50%, except that the short plug of alumina was not used. Elemental analysis of the product yielded satisfactory data.

[Ru(C_5H_5){η^6-$C_6H_5OCH(C_2H_5)(C_6H_{13})$}][$Tf_2N$] (*rac*-[1][$Tf_2N$]). This compound was synthesized as described for *rac*-[**1**][FSA], using [Ru(C_5H_5){η^6-$C_6H_5OCH(C_2H_5)(C_6H_{13})$}][$PF_6$] (162 mg, 0.30 mmol) and Li[Tf_2N] (175 mg, 0.61 mmol). The product was obtained as a pale yellow liquid (104 mg, 52% yield). ^{1}H NMR (400 MHz, $CDCl_3$): δ = 0.92 (t, 6H, CH_3, J = 7.0 Hz), 1.24–1.36 (m, 8H, CH_2), 1.60–1.66 (m, 4H, CH_2), 4.21–4.24 (m, 1H, ArOCH), 5.33 (s, 5H, Cp–H_5), 5.91 (t, 1H, Ar–H_1, J = 5.4 Hz), 6.10–6.16 (m, 4H, Ar–H_4). IR (ATR, cm^{-1}): ν = 1349, 1259, 1180, 1133, 1052, 634, 600, 570. Anal. Calcd. for $C_{22}H_{29}F_6NO_5RuS_2$: C, 39.64; H, 4.38; N, 2.10. Found: C, 39.71; H, 4.32; N, 2.13.

Synthesis of [Ru(C_5H_5){η^6-$C_6H_5OCH(C_4H_9)_2$}]X ([2]X; X = PF_6^-, FSA^-, Tf_2N^-)

[Ru(C_5H_5){η^6-$C_6H_5OCH(C_4H_9)_2$}][PF_6] ([2][PF_6]). Under a nitrogen atmosphere, (1-butylpentyl)oxy-benzene (133 mg, 0.60 mmol) was added to a solution of [Ru(C_5H_5)(CH_3CN)$_3$][PF_6] (219 mg, 0.50 mmol) in acetonitrile (10 mL), and the solution was stirred and maintained at 90 °C for 24 h. After evaporation of the solvent, the product was dissolved in dichloromethane and passed through a short plug of alumina (eluent: dichloromethane). After evaporation of the solvent, recrystallization from acetone and hexane (−40 °C) gave the desired compound as a white solid (162 mg, 61% yield). ^{1}H NMR (400 MHz, $CDCl_3$): δ = 0.93 (t, 6H, CH_3, J = 6.8 Hz), 1.26–1.36 (m, 8H,

CH_2), 1.61–1.66 (m, 4H, CH_2), 4.19–4.22 (m, 1H, ArOCH), 5.32 (s, 5H, Cp–H_5), 5.91 (t, 1H, Ar–H_1, J = 6.2 Hz), 6.08–6.13 (m, 5H, Ar–H_4). FT-IR (cm^{-1}): ν = 555, 823, 835, 1258. Anal. Calcd. for $C_{20}H_{29}F_6OPRu$: C,45.20; H, 5.50; N, 0.00. Found: C, 45.01; H, 5.31; N, 0.21.

[Ru(C_5H_5){η^6-$C_6H_5OCH(C_4H_9)_2$}][FSA] ([2][FSA]). This compound was synthesized as described for *rac*-[**1**][FSA], using [Ru(C_5H_5)(η^6-$C_6H_5OCH(C_4H_9)_2$)][PF_6] (350 mg, 0.66 mmol) and K[FSA] (433 mg, 1.98 mmol). The product was obtained as a pale yellow liquid (228 mg, 73% yield). ^{1}H NMR (400 MHz, $CDCl_3$): δ = 0.93 (t, 6H, CH_3, J = 7.0 Hz), 1.25–1.36 (m, 8H, CH_2), 1.61–1.66 (m, 4H, CH_2), 4.21–4.24 (m, 1H, ArOCH), 5.33 (s, 5H, Cp–H_5), 5.91 (t, 1H, Ar–H_1, J = 5.0 Hz), 6.10–6.14 (m, 5H, Ar–H_4). FT-IR (cm^{-1}): ν = 1380, 1362, 1258, 1178, 1102, 824, 732, 568. Anal. Calcd. for $C_{20}H_{29}F_2NO_5RuS_2$: C, 42.39; H, 5.16; N, 2.47. Found: C, 42.61; H, 5.42; N, 2.43.

[Ru(C_5H_5){η^6-$C_6H_5OCH(C_4H_9)_2$}][Tf_2N] ([2][Tf_2N]). This compound was synthesized as described for *rac*-[**1**][FSA], using [Ru(C_5H_5){η^6-$C_6H_5OCH(C_4H_9)_2$}][PF_6] (185 mg, 0.35 mmol) and Li[Tf_2N] (200 mg, 0.70 mmol). The product was obtained as a pale yellow liquid (88.1 mg, 38% yield). ^{1}H NMR (400 MHz, $CDCl_3$): δ = 0.92 (t, 6H, CH_3, J = 7.0 Hz), 1.24–1.36 (m, 8H, CH_2), 1.60–1.66 (m, 4H, CH_2), 4.21–4.24 (m, 1H, ArOCH), 5.33 (s, 5H, Cp–H_5), 5.91 (t, 1H, Ar–H_1, J = 5.4 Hz), 6.10–6.16 (m, 5H, Ar–H_4). FT-IR (cm^{-1}): ν = 1349, 1331, 1180, 1133, 1052, 614, 600, 569. Anal. Calcd. for $C_{22}H_{29}F_6NO_5RuS_2$: C, 39.64; H, 4.38; N, 2.10. Found: C, 39.71; H, 4.32; N, 2.13.

Synthesis of [Ru(C_5H_5)(η^6-$C_6H_5OC_9H_{19}$)]X ([3]X; X = PF_6^-, FSA^-, Tf_2N^-)

[Ru(C_5H_5)(η^6-$C_6H_5OC_9H_{19}$)][PF_6] ([3][PF_6]). This compound was synthesized as described for [**2**][PF_6], using [Ru(C_5H_5)($NCCH_3$)$_3$][PF_6] (203 mg, 0.47 mmol) and nonyloxybenzene (123 mg, 0.56 mmol). The product was obtained as white solid (221 mg, 89% yield). ^{1}H NMR (400 MHz, $CDCl_3$):

δ = 0.89 (t, 3H, CH_3, J = 6.8 Hz), 1.21–1.28 (m, 12H, CH_2), 1.72–1.76 (m, 2H, CH_2), 3.94 (t, 1H, ArOCH_2, J= 6.2 Hz), 5.35 (s, 5H, Cp–H_5), 5.93 (t, 1H, Ar–H_1, J = 5.6 Hz), 6.10 (t, 2H, Ar–H_2, J = 6.2 Hz), 6.16 (d, 2H, Ar–H_2, J = 6.4Hz). FT-IR (cm^{-1}): ν = 556, 824, 1257. Anal. Calcd. for $C_{20}H_{29}F_6OPRu$: C, 45.20; H, 5.50; N, 0.00. Found: C, 45.01; H, 5.29; N, 0.10.

[Ru(C_5H_5)(η^6-$C_6H_5OC_9H_{19}$)][FSA] ([3][FSA]). [Ru(C_5H_5)(η^6-$C_6H_5OCH(C_4H_9)_2$)][PF_6] (100 mg, 0.19 mmol) was dissolved in a mixture of water and acetone. An aqueous solution of K[FSA] (124 mg, 0.56 mmol) was added to this solution and the solution was stirred for 5 min. After evaporation of the acetone, the resulting suspension was extracted five times with dichloromethane. The product was dissolved in acetonitrile and passed through a short alumina plug (eluent: acetonitrile). The product was dissolved in a small amount of acetone, to which diethyl ether was added. Storage of the solution at −40 °C precipitated the desired compound as a white solid (60 mg, 56% yield). ^{1}H NMR (400 MHz, $CDCl_3$): δ = 0.89 (t, 3H, CH_3, J = 6.7 Hz), 1.28–1.40 (m, 12H, CH_2), 1.72–1.77 (m, 2H, CH_2), 3.95 (t, 1H, ArOCH_2, J = 6.4 Hz), 5.36 (s, 5H, Cp–H_5), 5.92 (t, 1H, Ar–H_1, J = 5.6 Hz), 6.12 (t, 2H, Ar–H_2, J = 6.0 Hz), 6.18 (d, 2H, Ar–H_2, J = 6.0 Hz). FT-IR (cm^{-1}): ν = 1379, 1366, 1255, 1181, 1101, 847, 824, 811, 724, 569. Anal. Calcd. for $C_{20}H_{29}F_2NO_5RuS_2$: C, 42.39; H, 5.16; N, 2.47. Found: C, 42.65; H, 4.99; N, 2.42.

[Ru(C_5H_5)(η^6-$C_6H_5OC_9H_{19}$)][Tf_2N] ([3][Tf_2N]). This compound was synthesized as described for *rac*-[**1**][FSA], using [Ru(C_5H_5)(η^6-$C_6H_5OC_9H_{19}$)][PF_6] (300 mg, 0.56 mmol) and Li[Tf_2N] (324 mg, 1.13 mmol). The product was obtained as a pale yellow liquid (256 mg, 68% yield). ^{1}H NMR (400 MHz, $CDCl_3$): δ = 0.88 (t, 3H, CH_3, J = 6.8 Hz), 1.21–1.28 (m, 12H, CH_2), 1.70–1.75 (m, 2H, CH_2), 3.93 (t, 1H, ArOCH_2, J= 6.2 Hz), 5.35 (s, 5H, Cp–H_5), 5.91 (t, 1H, Ar–H_1, J = 5.4 Hz), 6.12 (t, 2H, Ar–H_2, J = 6.0 Hz), 6.18 (d, 2H, Ar–H_2, J = 6.4Hz). FT-IR (cm^{-1}): ν = 1349, 1180, 1133, 1052, 614, 600, 569. Anal. Calcd. for $C_{22}H_{29}F_6NO_5RuS_2$: C, 39.64; H, 4.38; N, 2.10. Found: C, 40.04; H, 4.08; N,

2.18.

X-ray crystallography

Single crystals of [**2**][PF_6], [**3**][PF_6], and [**3**][FSA] were grown by slow evaporation of methanol solutions of the salts. X-ray diffraction data were collected by using a Bruker APEX II Ultra CCD diffractometer with Mo$K\alpha$ radiation (λ = 0.71073 Å) at 100 K. All calculations were done with SHELXTL. The structures were solved by direct methods (SHELXL 97).[40] Ortep-3 for Windows[41] was used to produce the molecular graphics. The crystallographic parameters are listed in Table S4 (ESI).

Acknowledgments

This work was financially supported by KAKENHI (grant numbers 24350073 and 26104524) from the Japan Society for the Promotion of Science (JSPS).

References

[1] A. Stark and K. R. Seddon, *Kirk-Othmer Encyclopedia of Chemical Technology*, 2007, **26**, 836–920.

[2] H. Tokuda, K. Hayamizu, K. Ishii, Md. A. B. H. Susan and M. Watanabe, *J. Phys. Chem. B*, 2005, **109**, 6103–6110.

[3] J. D. Holbrey and K. R. Seddon, *J. Chem. Soc., Dalton Trans.*, 1999, 2133–2139.

[4] M. Iida, C. Baba, M. Inoue, H. Yoshida, E. Taguchi and H. Furusho, *Chem. Eur. J.*, 2008, **14**, 5047–5056.

[5] M. Iida, S. Kawakami, E. Syouno, H. Er and E. Taguchi, *J. Colloid Interface Sci.*, 2011, **356**, 630–638.

[6] T. Erdmenger, J. Vitz, F. Wiesbrock and U. S. Schubert, *J. Mater. Chem.*, 2008, **18**, 5267–5273.

[7] A. Andresova, J. Storch, M. Traïkia, Z. Wagner, M. Bendova, P. Husson, *Fluid Phase Equilib.*, 2014, **371**, 41–49.

[8] M. Lartey, J. Meyer-Ilse, J. D. Watkins, E. A. Roth, S. Bowser, V. A. Kusuma, K. Damodaran, X. Zhou, M. Haranczyk, E. Albenze, D. R. Luebke, D. Hopkinson, J. B. Kortright and H. B. Nulwala,

Phys. Chem. Chem. Phys., 2015, **17**, 29834–29843.

[9] Y. Zhang, L. Xue, F. Khabaz, R. Doerfler, E. L. Quitevis, R. Khare and E. J. Maginn, *J. Phys. Chem. B*, 2015, **119**, 14934−14944.

[10] L. Pison, K. Shimizu, G. Tamas, J. N. Canongia Lopes, E. L. Quitevis and M. F. Costa Gomes, *Phys. Chem. Chem. Phys.*, 2015, **17**, 30328–30342.

[11] H. K. Kashyap, C. S. Santos, N. S. Murthy, J. J. Hettige, K. Kerr, S. Ramati, J. Gwon, M. Gohdo, S. I. Lall-Ramnarine, J. F. Wishart, C. J. Margulis and E. W. Castner, *J. Phys. Chem. B*, 2013, **117**, 15328−15337.

[12] Y. Yoshida and G. Saito, in *Ionic Liquids: Theory, Properties, New Approaches*, ed. A. Kokorin, INTECH, 2011, ch. 29, pp. 723–738.

[13] P. Zhang, Y. Gong, Y. Lv, Y. Guo, Y. Wang, C. Wang and H. Li, *Chem. Commun*., 2012, **48**, 2334–2336.

[14] J. Klingele, *Coord. Chem. Rev.*, 2015, **292**, 15–29.

[15] I. J. B. Lin and C. S. Vasam, *J. Organomet. Chem*., 2005, **690**, 3498–3512.

[16] N. R. Brooks, S. Schaltin, K. Van Hecke, L. Van Meervelt, K. Binnemans and J. Fransaer, *Chem. Eur. J.*, 2011, **17**, 5054–5059.

[17] T. Inagaki, T. Mochida, M. Takahashi, C. Kanadani, T. Saito and D. Kuwahara, *Chem. Eur. J*., 2012, **18**, 6795–6804.

[18] Y. Funasako, T. Inagaki, T. Mochida, T. Sakurai, H. Ohta, K. Furukawa and T. Nakamura, *Dalton Trans*., 2013, **42**, 8317–8327.

[19] T. Inagaki and T. Mochida, *Chem.Eur. J.*, 2012, **18**, 8070–8075.

[20] A. Komurasaki, Y. Funasako and T. Mochida, *Dalton Trans*., 2015, **44**, 7595–7605.

[21] T. Ueda and T. Mochida, *Organometallics*, 2015, **34**, 1279−1286.

[22] F. A. Carey, *Organic Chemistry*, The McGraw-Hill Companies, USA, 4th ed. 2000.

[23] M. J. Hollamby and T. Nakanishi, *J. Mater. Chem. C*, 2013, **1**, 6178–6183.

[24] W. Pisula, M. Kastler, D. Wasserfallen, T. Pakula and K. Müllen, *J. Am. Chem. Soc*., 2004, **126**, 8074–8075.

[25] N. Ríos-Lombardía, E. Busto, V. Gotor-Fernández, V. Gotor, R. Porcar, E. García-Verdugo, S. V. Luis, I. Alfonso, S.Grancía-Granda and A. Menéndez-Velázquez, *Chem. Eur. J.*, 2010, **16**, 836–847.

[26] J. Jacques and A. Collet, S.H. Wilen, *Enantiomers, Racemates and Resolutions*, Krieger Pub. Co., 1994.

[27] T. Payagala and D.W. Armstrong, *Chirality*, 2012, **24**, 17–53.

[28] D. Turnbull and M. H. Cohen, *Modern Aspect of the Vitreous State*; Butterworth, London, 1960, **1**, 38.

[29] O. Yamamuro, Y. Minamimoto, Y. Inamura, S. Hayashi and H. Hamaguchi, *Chem. Phys. Lett.* 2006, **423**, 371−375.

[30] G. Annat, M. Forsyth and D. R. MacFarlane, *J. Phys. Chem. B*, 2012, **116**, 8251–8258.

[31] M. Kunze, S. Jeong, E. Paillard, M. Winter and S. Passerini, *J. Phys. Chem. C*, 2010, **114**, 12364–12369.

[32] H.-B. Han, S.-S. Zhou, D.-J. Zhang, S.-W. Feng, L.-F. Li, K. Liu, W.-F. Feng, J. Nie, H. Li, X.-J. Huang, M. Armand and Z.-B. Zhou, *J. Power Sources*, 2011, **196**, 3623–3632.

[33] A. Paul and A. Samanta, *J. Phys. Chem. B*, 2008, **112**, 16626–16632.

[34] H. Matsumoto, H. Sakaebe, K. Tatsumi, M. Kikuta, E. Ishiko and M. Kono, *J. Power Sources*, 2006, **160**, 1308–1313.

[35] M. Ishikawa, T. Sugimoto, M. Kikuta, E. Ishiko and M. Kono, *J. Power Sources*, 2006, **162**, 658–662.

[36] O. Borodin, W. Gorecki, G. D. Smith and M. Armand, *J. Phys. Chem. B*, 2010, **114**, 6786–6798.

[37] K. R. Harris, M. Kanakubo and L. A. Woolf, J. *Chem. Eng. Data*, 2007, **52**, 2425–2430.

[38] Y. Miura, F. Shimizu and T. Mochida, *Inorg. Chem.* 2010, **49**, 10032–10040.

[39] B.M. Trost and C. M. Older, *Organometallics* 2002**, 21**, 2544-2546.

[40] G. M. Sheldrick, *Acta Crystallogr*., 2008, **A64**, 112–122.

[41] L. J. Farrugia, *J. Appl. Crystallogr.*, 1997, **30**, 565.

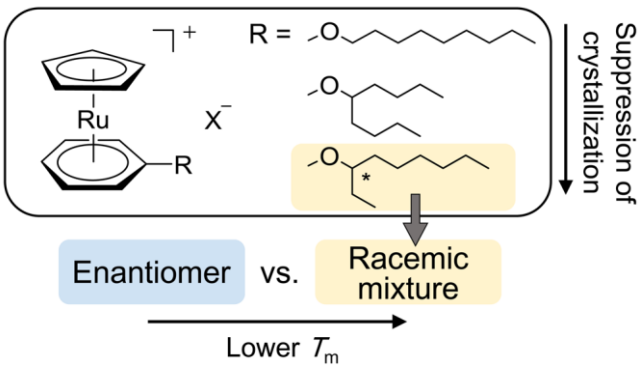

Organometallic ionic liquids with less symmetrical substituents tend to maintain the liquid state due to suppression of crystallization.

Supporting Information

Effects of substituent branching and chirality on physical properties of ionic liquids based on cationic ruthenium sandwich complexes

Tomomi Higashi, Takahiro Ueda, Tomoyuki Mochida*

Department of Chemistry, Graduate School of Science, Kobe University, Kobe, Hyogo 657-8501, Japan. E-mail: tmochida@platinum.kobe-u.ac.jp

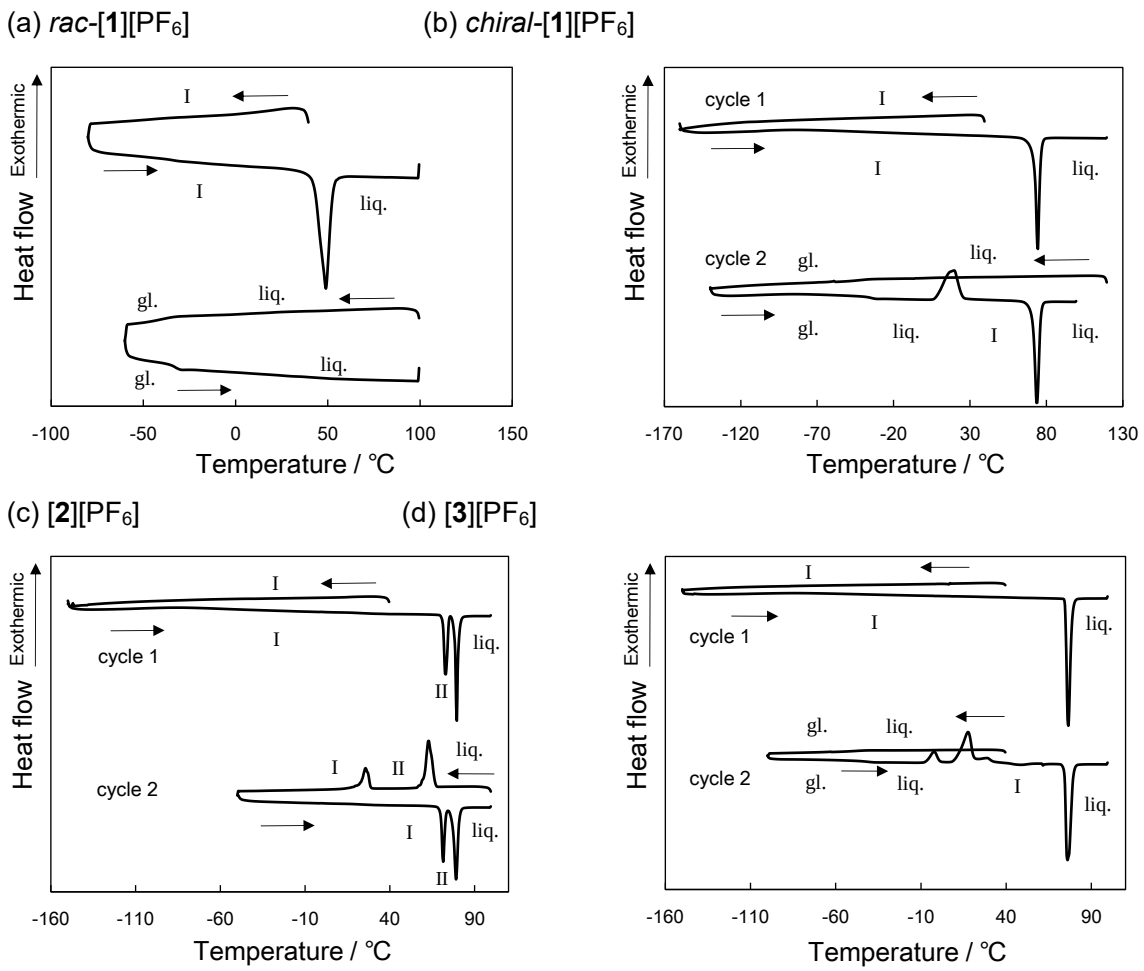

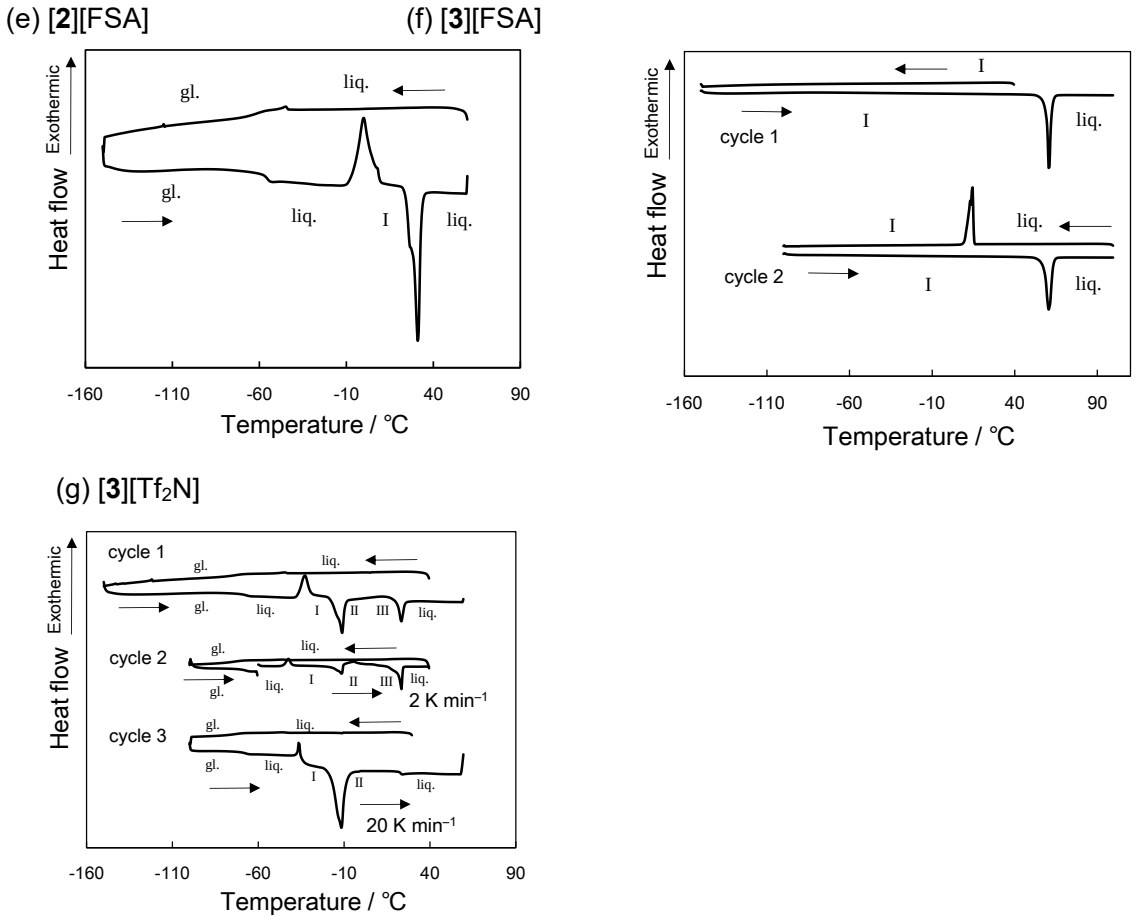

Fig. S1 DSC traces of salts that exhibited melting (*gl.*: glassy phase, *liq.*: liquid phase).

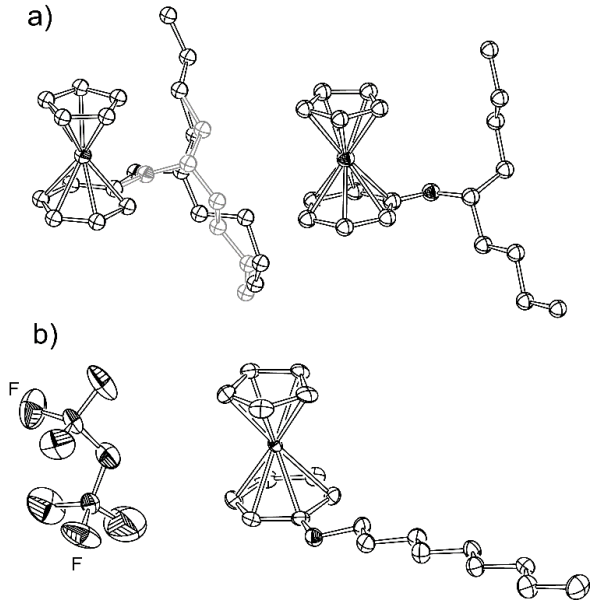

Fig. S2 Ortep diagrams of molecular structures of (a) [**2**][PF_6] and (b) [**3**][FSA]. One of the disordered parts in the substituent in [**2**][PF_6] is displayed in gray.

Table S1 Viscosity data (mPa s) for [**1**]X (X = PF_6, FSA, Tf_2N) and [**3**][Tf_2N]

°C	*rac*-[**1**][PF_6]	*rac*-[**1**][FSA]	*rac*-[**1**][Tf_2N]	[**3**][Tf_2N]
–20		40300	40300	9300
–15		23800	22200	5980
–10		13200	12100	3820
–5		7440	6850	2320
0		4710	4260	1580
5	248000	3020	2720	1090
10	118000	1970	1800	766
15	61900	1350	1220	543
20	33600	960	861	409
25	19600	700	623	312
30	11800	511	447	239
35	7420	381	336	187
40	5040	285	251	147
45	2840	221	189	115
50	1860	173	146	92

Table S2 Viscosity data (mPa s) for [**2**][FSA]

°C	[**2**][FSA]
–9	23800
–5	14700
–1	9680
5	5440
9	3790
15	2340
19	1700
25	1110
29	836
35	554
39	430
45	292
50	218

Table S3 Viscosity data (mPa s) for [**2**][Tf_2N]

°C	[**2**][Tf_2N]
–20	87200
–16	47100
–10	21100
–6	13000
0	6860
4	4260
10	2410
14	1740
20	1100
25	775
30	549
34	428
40	296
44	236
50	172

Table S4 Crystallographic parameters

	[**2**][PF_6]	[**3**][PF_6]	[**3**][FSA]
Empirical formula	$C_{20}H_{29}F_6OPRu$	$C_{20}H_{29}F_6OPRu$	$C_{20}H_{29}F_2NO_5RuS_2$
Formula weight	531.47	531.47	566.63
Crystal system	Triclinic	Triclinic	Triclinic
Space group	*P*–1	*P*–1	*P*–1
a (Å)	7.2400(9)	10.389(3)	7.928(3)
b (Å)	18.137(2)	10.393(3)	9.542(4)
c (Å)	18.786(2)	11.050(3)	16.403(6)
α (°)	114.7030(10)	84.703(4)	98.073(5)
β (°)	94.018(2)	67.159(4)	101.571(4)
γ (°)	97.896(2)	82.242(4)	103.610(4)
Volume (Å^3)	2197.4(5)	1088.4(5)	1158.3(8)
Z	4	2	2
$d_{calcd.}$ (mg m^{-3})	1.606	1.622	1.625
T (K)	100	100	100
μ (mm^{-1})	0.845	0.853	0.904
Reflections collected	10721	5053	5408
Independent reflections	7656 (R_{int} =0.0204)	3740 (R_{int} = 0.0162)	4022 (R_{int} = 0.0260)
F(000)	1080	540	580
R_1[a], wR_2[b] ($I > 2\sigma$(I))	0.0258, 0.0656	0.0256, 0.0579	0.0577, 0.1556
R_1[a], wR_2[b] (all data)	0.0286, 0.0679	0.0292, 0.0597	0.0610, 0.1629
Goodness-of-fit on F^2	1.038	1.060	1.114
Completeness to θ (%)	98.3	97.3	98.0
Parameters	587	263	281
Largest diff. peak and hole	1.040 and −0.562	0.554 and −0.473	2.362 and −1.235

[a] $R_1 = \Sigma \, ||F_o| - |F_c|| \, / \, \Sigma \, |F_o|$, b) $wR_2 = [\, \Sigma \, w(F_o^2 - F_c^2)^2 \, / \, \Sigma \, w(F_o^2)^2]^{1/2}$